AD-A064 742 BRISTOL UNIV (ENGLAND) H H WILLS PHYSICS LAB F/G 13/5
STATES OF STRESS AND STRAIN IN ADHESIVE JOINTS.(U)
SEP 78 N R FARRAR, K H ASHBEE AFOSR-77-3448

UNCLASSIFIED AFOSR-TR-79-0066 NL

1 OF 1
AD
A064742

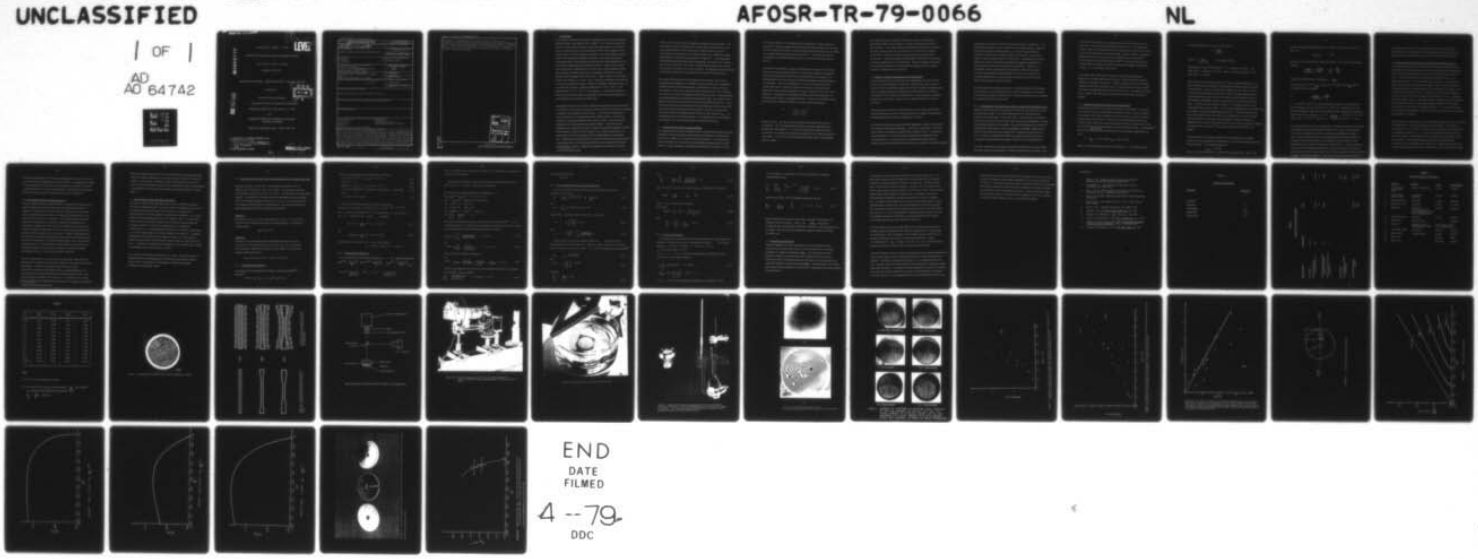

END
DATE
FILMED
4 -79
DDC

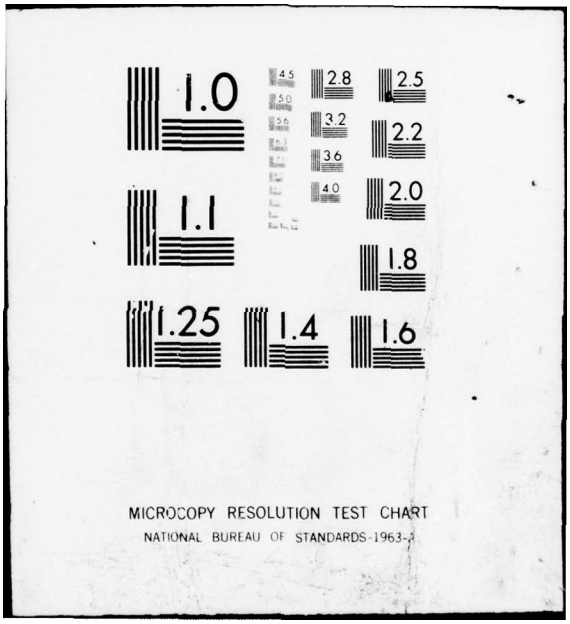
1.0
1.1
1.25
1.4
1.6
1.8
2.0
2.2
2.5
2.8
3.2
3.6
4.0
4.5
5.0
5.6
MICROCOPY RESOLUTION TEST CHART
NATIONAL BUREAU OF STANDARDS-1963-A

AFOSR-TR- 79-0066

LEVEL

AD A064742

Grant Number: AFOSR - 77 -3448

STATES OF STRESS AND STRAIN IN ADHESIVE JOINTS

N.R. Farrar and K.H.G. Ashbee

September 29th 1978

Interim Scientific Report, September 30th 1977 - September 29th 1978

DDC
FEB 21 19
A

prepared for

UNITED STATES AIR FORCE

AIR FORCE OFFICE OF SCIENTIFIC RESEARCH

Building 410, Bolling Air Force Base, D.C. 20332

and

EUROPEAN OFFICE OF AEROSPACE RESEARCH
AND DEVELOPMENT

223/231 Old Marylebone Road, London NW1 5TH

DDC FILE COPY

AIR FORCE OFFICE OF SCIENTIFIC RESEARCH (AFSC)
NOTICE OF TRANSMITTAL TO DDC
This technical report has been reviewed and is
approved for public release IAW AFR 190-12 (7b).
Distribution is unlimited.
A. D. BLOSE
Technical Information Officer

Approved for public release;
distribution unlimited.

79 02 16 006

UNCLASSIFIED

SECURITY CLASSIFICATION OF THIS PAGE (When Data Entered)

REPORT DOCUMENTATION PAGE

READ INSTRUCTIONS BEFORE COMPLETING FORM

1. REPORT NUMBER: AFOSR-TR-79-0066	2. GOVT ACCESSION NO.
3. RECIPIENT'S CATALOG NUMBER	
4. TITLE (and Subtitle): STATES OF STRESS AND STRAIN IN ADHESIVE JOINTS.	5. TYPE OF REPORT & PERIOD COVERED: INTERIM, 30 Sep 77 - 28 Sep 78
	6. PERFORMING ORG. REPORT NUMBER
7. AUTHOR(s): N. R. FARRAR, K. H. G. ASHBEE	8. CONTRACT OR GRANT NUMBER(s): AFOSR-77-3448
9. PERFORMING ORGANIZATION NAME AND ADDRESS: UNIVERSITY OF BRISTOL, H H WILLS PHYSICS LABORATORY/ROYAL FORT, TYNDALL AVENUE, BRISTOL BS8 1TL	10. PROGRAM ELEMENT, PROJECT, TASK AREA & WORK UNIT NUMBERS: 2307B2, 61102F
11. CONTROLLING OFFICE NAME AND ADDRESS: AIR FORCE OFFICE OF SCIENTIFIC RESEARCH/NA, BLDG 410, BOLLING AIR FORCE BASE, D C 20332	12. REPORT DATE: 29 Sep 78
	13. NUMBER OF PAGES: 43
14. MONITORING AGENCY NAME & ADDRESS (if different from Controlling Office): 45p.	15. SECURITY CLASS. (of this report): UNCLASSIFIED
	15a. DECLASSIFICATION/DOWNGRADING SCHEDULE

16. DISTRIBUTION STATEMENT (of this Report)

Approved for public release; distribution unlimited.

17. DISTRIBUTION STATEMENT (of the abstract entered in Block 20, if different from Report)

18. SUPPLEMENTARY NOTES

19. KEY WORDS (Continue on reverse side if necessary and identify by block number)

ADHESIVE JOINTS
ALUMINIUM
WATER UPTAKE
SWELLING
STRESS ENHANCED MIGRATION OF WATER
NEWTON'S RINGS
NON-FICKIAN DIFFUSION
SELF-STRESSED FRACTURE MECHANICS

20. ABSTRACT (Continue on reverse side if necessary and identify by block number)

The swelling during water uptake by adhesive joints is strongly inhomogeneous. In particular, there exists a well defined shoulder between fully saturated and less than fully saturated adhesive. The pricipal stresses, introduced as a consequence of the mechanical constraint exerted by the adherends, include a normal stress that is compressive near the rim of the adhesive layer and tensile near its center. The magnitude of this stress has been measured, for joints involving aluminium as one adherend and a microscope cover slip as the other adherend by analyzing the pattern of Newton's rings created between the cover slip and on optical flat. Near

DD FORM 1 JAN 73 1473 393 113

UNCLASSIFIED

the shoulder, the normal stress is of the order of a kilobar and this is estimated to be large enough to significantly enhance water migration and hence explain certain non-Fickian behaviors that have also been observed. The groundwork has been completed for development of a self-stressed mode I fracture mechanics test-piece. Geometrically, the test-piece is simply a disclination in a disc of the adherend metal.

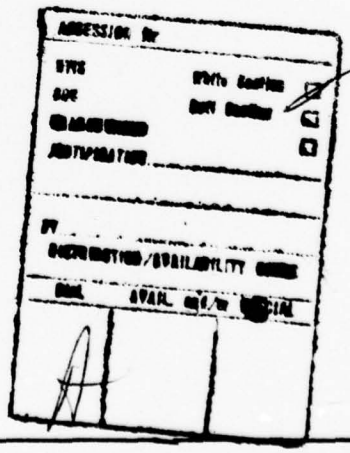

1. Introduction

In the course of research subsequently supported by the US Army European Research Office under grant No. DA - ERO - 76 - G - 068, an attempt was made to measure water migration rates within and parallel to resin layers that are sufficiently thin to be representative of the resin trapped between adjacent fibres in FRP*. Samples of polyester resins and samples of epoxy resins, both containing entrapped air bubbles, were cast between glass microscope slides, cured in strict accordance with recommendations by the respective manufacturers and immersed in water. Rates of water uptake were measured by noting the times at which water droplets appeared inside the entrapped air bubbles which were conveniently distributed at various distances from the edge of each resin layer. Figure 1 shows water droplets inside an air bubble in an epoxy joint. The data so obtained, and reported in a seminar presented by K. H. G. Ashbee at AMMRC, Watertown, Mass. on July 23rd 1976, indicate diffusion coefficients of $\sim 10^{-4}$ cm^2 s^{-1} for polyesters and $\lesssim 10^{-7}$ cm^2 s^{-1} for epoxies, i.e. diffusion coefficients which are both about an order of magnitude faster than values published for water diffusion in the respective bulk resins.

The apparent enhancement of water migration through thin resin layers could be attributed to water flow through some kind of channels (crazes?) but evidence in support of this hypothesis was not found. An alternative explanation is that it could be due to attraction afforded by tensile stress. In a joint not subjected to externally applied stress, there are three mechanisms which might give rise to stress within the adhesive layer. The first of these, shrinkage that accompanies curing, is assumed to generate negligible residual stress because curing is carried out above T_g at which temperature it is expected that dimensional changes will be accommodated by viscoelastic flow. Differential contraction between resin and metal during cooling from the curing temperature will be partially relieved by self-adjustment of the glue line thickness. However, displacements parallel to the plane of the joint

* Fibre Reinforced Plastic

79 02 16 006

will not be so relieved and are expected to introduce lateral tensions. The third possible source of tensile stress within adhesive layers derives from water uptake. Adhesives swell during water uptake and since the water concentration is larger nearer the exposed surface, the swelling is strongly inhomogeneous as indicated schematically in Figure 2 B. As a consequence of mechanical constraint offered by the adherends, see Figure 3 B, adhesive near the rim of the joint is in a state of compression normal to the joint and resin nearer the centre is in a state of tension. Investigation and measurement of this effect constitutes the main thrust of the research reported herein.

Soon after commencement of this programme of research, the principal investigator participated in a workshop on structural adhesives, organised by AFOSR and held at Vought Corporation, Grand Prairie, Texas, December 5th & 6th 1977. Some of the formal presentations and much of the workshop time centred on fracture toughness testing of adhesive joints. Notwithstanding well founded attacks on the physical interpretation of K_{Ic} data collected from adhesive joints (the dilemma stems from the inescapable fact that very nearly all of the strain energy is stored by the metals joined and not by the adhesive), it became evident that an urgent need exists for a fracture mechanics test which lends itself to investigation of the effects of water uptake on K_{Ic}. As an additional task to the present project, it was decided to give some thought to development of a self-stressed fracture mechanics test-piece.

2. Use of Newton's rings to monitor swelling

The displacement normal to an adhesive layer is conveniently monitored during swelling by observing Newton's rings created by having one of the adherents thin so that it flexes, and in contact with a reference flat. A regular 150 μm thick microscope cover slip serves as the flexible adherend and the metal of interest, a slab of phosphoric acid anodised aluminium for example, is used

as the other adherend. The experimental arrangement is shown in Figure 4. Light from a mercury vapour lamp is directed through the optical flat, towards the cover slip and interference between incident and reflected beam occurs within the variable thickness gap located between the two. The Newton's rings are photographed using light reflected into a 35 mm camera by the half silvered mirror.

The pattern of interference fringes is determined by the geometry of the gap between cover slip and optical flat and, to ensure that changes in the pattern arise only from distortion of the cover slip caused by resin swelling, it is essential that each run be carried out without disturbing the specimen/optical flat assembly. All of the components are set up on an optical bench and, for hot water tests, it has been necessary to develop a rig which avoids condensation on the optical components. Figure 5 shows the mark I hot water apparatus. Development of this apparatus demonstrated the importance of minimising the number of air/glass interfaces. Table 1 lists calculated values for the reflection coefficient (R) for the various interfaces present.

$$R = \left(\frac{n_2 - n_1}{n_2 + n_1} \right)^2$$

where n_1 and n_2 are the refractive indices of the materials in contact at an interface. The $\lambda/10$ optical flats used for the present experiments are ground from crown glass ($n = 1.5$) and the intensity lost by reflection at the air interface is too large for satisfactory resolution of the fringes produced by some joints. This loss can be minimised by inserting a film of intermediate refractive index.

In its simplest form, the pattern of Newton's rings is a consequence of interference between just two beams, namely the incident beam and the reflected beam. The fringe contrast is considerably enhanced by silvering the upper surface of the cover slip and the lower surface of the optical flat in order to produce multiple reflections and hence multiple beam interference. To permit transmission through the optical flat, only partial silvering is admissible for this component. Superior fringes are obtained, cf. (a) and (b) in Figure 6, but the problem of depositing water resistant reflective coatings has yet to be solved.

2.1 Materials, surface treatments and joint preparation

The first long term test was made at room temperature on a joint between a cover slip and cleaned,but not anodised, S1C aluminium and, in order to make use of data mentioned on page 1 of this report, a general purpose epoxy resin containing entrapped air bubbles was used as adhesive. Hereafter, this adhesive will be referred to as adhesive A. Its full identity, including hardener and accelerator, and the curing schedule used for it are given in Table 2.

Later tests were carried out on joints between a cover slip and substrates on both S1C aluminium and E N 58 stainless steel, using the commercially available adhesive film system designated B in Table 2.

All metal surfaces were cleaned and, where applicable, treated in accordance with commercially accepted practice. In the case of aluminium, the normal US procedure is attributed to Miller[1] and is listed in Table 3. A somewhat similar procedure, but with a chromic acid instead of a phosphoric acid anodising solution, is used in the UK by Westland Helicopters Limited. Aluminium adherends prepared by each method were used for the present studies.

Preparation of the glass cover slip surfaces is less well standardised. The fundamental problem is removal of oxides of low surface energy. Chemical attack by the common oxidising agents, e.g. nitric acid and hydrogen peroxide certainly remove a large fraction of these oxides. So too does exposure to the oxidising region of a naked flame. Sand blasting in order to roughen the surface and promote mechanical linkages, and application of coupling agents (silanes) have also been recommended. However, no combination of these treatments has yet produced a joint which, when it eventually debonds after prolonged exposure to water in the absence of externally applied stress, leaves fracture surfaces which do not include larger areas of glass adhesive interface.

In joints manufactured using liquid resin, a reproducible glue line thickness was achieved by simply allowing the cover slip to sink under its own weight. In joints made using solid adhesive film, the glue line thickness was controlled by clamping during the cure process.

2.2. Interpretation of characteristic features in the pattern of Newton's rings

Adjacent rings of the same colour (black or white) are loci of points for which the optical path length, in the space between cover slip and optical flats, differs by one wavelength. By the same token, a displacement in the pattern of Newton's rings by an amount equal to one ring width corresponds to a change in path length equal to one wavelength. By observing changes in the number of rings between fixed markers, such as entrapped air bubbles, displacements normal to the joint during water uptake can be measured to an accuracy of $\lambda/4$. If required, displacements which are at least as small as $\lambda/10$ can be measured by superimposition of images in order to create Moiré patterns.

The water concentration, and hence the swelling associated with water uptake, eventually saturates and thereafter a shoulder separating fully saturated from

less than fully saturated resin, progressively moves inwards from the rim of the joint. This is shown schematically in Figure 2 C. The shoulder is clearly resolved in the pattern of Newton's rings since it gives rise to a locus of kinks in the individual interference fringes. Figure 7 shows a sequence of images obtained from an aluminium joint manufactured with adhesive A and immersed in static distilled water at 20°C; The locus of kinks is best resolved where the fringe orientation is such that the change in orientation is large, e. g. at B in Figure 7(a) and (c).

To maintain contact with the outer ring of uniformly swollen adhesive (Figure 3C), the adherends would each need to bend with curvature that is opposite to that inside the shoulder. Failure to adopt such "S" wise bending manifests itself as an interfacial crack, the occurrence of which is revealed as patches of bright contrast at the rim in Figure 7(c). The patches eventually link up, Figure 7(d), and produce resolvable circumferential interference fringes.

2. 3. Analysis of data from Newton's rings experiments

Displacement normal to the joint of one quarter of a wavelength is revealed as a reversal of contrast in the pattern of Newton's rings. Thus the bright → dark change at the fringe indicated by arrow A in Figure 7 (a) → (c) indicates a displacement of 136. 5 nm (λ = 546. 1 nm for the green light emitted by the mercury vapour lamp used in the present experiments) at a point 6mm in from the rim after only two weeks exposure to room temperature water. Timoshenko's[2] formula for the axial stress σ produced by an axial load W on a thin plate supported at its rim is

$$\sigma = \frac{W}{h^2} \left[(1 + \nu) (0.4851 n \frac{a}{h} + 0.52) + 0.48 \right]$$

where h is the plate thickness and 2a is its diameter. ν is Poisson's ratio.

The axial displacement ω is given by Love[3] as

$$\omega = \frac{Wa^2}{16 \pi D}$$

where $D = \frac{Eh^3}{12 (1 - \nu^2)}$ E is Young's modulus

Substituting $E = 6.3 \times 10^{11}$ dynes cm^{-2}, $\nu = 0.25$ and $h = 150 \mu m$, it is found that $D = \sim 10^5$ ergs. $2a = 19$ mm. Hence, $\omega = 136.5$ nm gives $W = 144$ dynes and $\sigma = 2.33$ bars.

This estimate for σ assumes that the cover slip is rigidly clamped at its rim but is otherwise free to undergo a dome-shaped deformation under the action of axial load W. In fact, the cover slip is bonded over the whole of its area of contact with the adhesive and the deformation is strongly inhomogeneous, being concentrated in the vicinity of the shoulder between adhesive which is fully saturated and adhesive which is less than fully saturated with diffused water. Across the locus of kinks in Figure 7, the fringe deviation amounts to approximately two ring widths, i.e. to a normal displacement of λ (0.5461 μ m) in an annular ring width of approximately 0.8 mm. A local thickening of the 15 μ m thick adhesive film by 0.5461 μ m corresponds to a linear swelling of almost 4% which is close to the value expected for saturated swelling. A displacement of 0.5461 μ m normal to a 0.8 mm wide ribbon of glass corresponds to a shear strain of nearly 10^{-2} and hence to a local stress of about two kilobars.

A rough estimate of the stress required for stress induced drift of water molecules to be as important as diffusion down a concentration gradient may be made as follows. The respective fluxes are

$$j_{drift} = -\mu c \nabla \phi$$

where μ is the drift mobility, c is the water concentration and $\nabla \phi$ is the

potential energy gradient arising from the tensile stress at the middle of the joint, and

$$j_{\text{diffusion}} = - D \nabla c$$

where D is the water diffusion coefficients and ∇c is the water concentration gradient.

$$\frac{j \text{ drift}}{j \text{ diffusion}} = \frac{\mu c \nabla \phi}{D \nabla c} = \frac{c}{\nabla c} \frac{\nabla \phi}{kT}$$

using the Nernst-Einstein relationship $\mu = \frac{D}{k T}$.

The dimensions are cm for $\frac{c}{\nabla c}$ and erg cm^{-1} for $\nabla \phi$. Hence $\frac{c}{\nabla c} \nabla \phi$ is a quantity of energy, say $\Delta \phi$.

i.e. $$\frac{j \text{ drift}}{j \text{ diffusion}} \sim \frac{\Delta \phi}{k T}$$

$k = 1.4 \times 10^{-16}$ erg K^{-1} so, for the fluxes to be equal at room temperature, $\Delta \phi$ would have to be of the order of 4.2×10^{-14} erg. Assuming that water molecules migrate singly and cause swelling equal in magnitude to the natural volume of the water molecule, i.e. $\Delta V = \frac{18}{6 \times 10^{23}} = 30 \times 10^{-24}$ cm^3, then $\Delta \phi = p \Delta V = 4.2 \times 10^{-14}$ ergs and $p = 1.4 \times 10^{9}$ dynes $cm^{-2} \sim 1$ kbar.

Very similar results have been obtained from changes in the pattern of Newton's rings observed during water uptake by adhesive B. That is, displacements remote from the edge of the joint occur after surprisingly short exposure times, large displacements and correspondingly large stresses straddle the boundary between fully swollen and less than fully swollen adhesive, and debonding at the rim follows attainment of full saturation. These conclusions are true for joints manufactured between a glass cover slip as one adherend and aluminium, both with and without either of the anodising treatments described on page 4, as the other adherend. Use of hot water rather than cold water as

the exposure medium merely accelerates incidence of the phenomena reported above. An insight into the kinetics governing these phenomena is provided by these accelerated tests and will be examined in section 2.4.

2.4 Kinetics of processes arising from water uptake by adhesive joints

The spatial positions of the locus of kinks in the pattern of Newton's rings, of the edge of the debonding crack and of water droplets inside entrapped air bubbles are all very well defined and have been measured as functions of time. The data obtained from the experiment reported in figure 7 are presented in Figure 8. To test whether any of the data fit the solution to Fick's law for the case of a planar interface between infinitely long bars of solution and solvent, published by Barrer[4] for example, the measurements are plotted as functions of $(\text{time})^{\frac{1}{2}}$. Migration of the shoulder defining the extent of water saturation is evidently not controlled by a $t^{\frac{1}{2}}$ law. Migration of the crack edge, however, does approximate reasonably well to $t^{\frac{1}{2}}$ behaviour. The kink selected because of its sharp change in direction at the shoulder did not fall on a radius where debonding initiated, i.e. the two sets of data are for different radii and the cross-over does not indicate that the crack edge has overtaken the shoulder.

The data shown in Figure 9 are for a joint manufactured between a cover slip and a microscope slide and described on page 1 of this report. The adhesive is that referred to as A in Table 2, and the immersion medium was boiling water. A reasonably straight line, i.e. a $t^{\frac{1}{2}}$ law, can be drawn through each of the three sets of data. The change from $t^{\frac{1}{2}}$ to t behaviour for the shoulder could be attributed to plasticisation causing lowering of the glass transition temperature to below boiling water temperature. Formulation A (Table 2) is a general purpose epoxy resin that is widely used as the matrix phase in FRP.

Dissolution by diffused water of water solubles present as impurities in this resin creates penny-shaped pressure filled voids[5], the appearance of which at various distances from the free surface provides yet another method for measuring kinetics for a water uptake process. Such data for bulk samples immersed in boiling water are strictly linear with time, Figure 10.

2.5 Discussion of Newton's rings experiments

If water migration within the adhesive layer is significantly enhanced by the self-stressing that evidently results from the inhomogeneous nature of swelling, it follows that the effective diffusion coefficient is a function of water concentration and processes occurring at rates proportional to the square root of time cannot be expected. The self generation of high local stresses during swelling is a property of adhesives and appears to be unaffected by changing the materials used as adherends or by the surface treatments applied to adherends in order to resist mechanical failure when external forces are applied to the joint itself. Complete understanding of the problem will require investigation into the nature of swelling and areas of research fundamental to this include identification of the various states of diffused water, the mechanism(s) by which diffused water promotes so-called plasticisation, and the precise origin(s) of dimensional changes attributable to curing , water uptake and water expulsion.

As far as continuation of the present work is concerned, joints involving stainless steel, titanium or carbon fibre reinforced resins have not yet been investigated. From the conclusions drawn here from the data obtained from aluminium adherends and from all-glass adherends, it is anticipated that strongly inhomogeneous swelling of adhesive occurs in all joints and causes enhanced water migration. It is possible that, in joints involving CFRP* water diffusion into the adherend will mitigate this process.

* Carbon Fibre Reinforced Plastic

Data are being generated for the rates at which various processes dependant upon water uptake actually occur, and these data are amenable to empirical analysis. For example, debonding of joints in boiling water is faster by a factor of 40 than debonding of joints in room temperature water, and assumption that debonding is thermally activated yields an activation energy of ~ 5 Kcal $mole^{-1}$.

3. Self-stressed fracture mechanics test-piece

Professor W. Harris from the department of micro-molecular mechanics, University of Witwatersrand[6], has coined the term "dispiration" to describe the most general line defect that can be conceived. Introduction of a dispiration into a solid would generate rotation plus translation, i.e. it would produce a helical displacement; hence the syllable...spir...to infer spiral. A line defect which introduces rotation only is known as a disclination and one which introduces a rigid body translation only is a dislocation.
A disclination, i.e. a line defining the termination of a rotation, is generated in, say a disc-shaped solid, by forcing a wedge into a radial cut. An opposite disclination would be generated by making two radial cuts, removing the wedge thereby produced, and forcing the exposed faces into contact with each other. By bonding (or welding) the faces together a self-stressed disc, capable of propagating a pure mode I crack, is created.

The calculation given below is by Professor J. Tweed of the Department of Mathematical and Computing Sciences, Old Dominion University, Norfolk, Virginia and is the outcome of correspondence between the principal investigator and Professor Tweed.

3.1 The plane elastic problem for a self-stressed disc with a radial edge crack

Consider in figure 11 a disc which, in plane polar coordinates (r, θ), is defined by the relations $0 \leq r \leq a$, $0 \leq \theta \leq 2\pi$. Let the disc be stressed by removing a sector $0 \leq r \leq a$, $2\pi - \Omega < \theta < 2\pi$ and joining the resulting edges together. The problem to be solved is that of calculating the stress intensity factor and formation energy of a crack $a\,c \leq r \leq a$, $\theta = 0$ in this disc under the assumption that plane stress conditions exist. We solve the problem by superimposing the solutions of problems 1 and 2 below.

Problem 1

In the disc $0 \leq r \leq a$, $0 \leq \theta \leq 2\pi$ the sector $0 \leq r \leq a$, $2\pi - \Omega < \theta < 2\pi$ is removed and the surfaces thus formed are joined together. Calculate the resulting stress

$$\sigma_{\theta\theta}\ (r, 0) = \sigma\ (r).$$

Problem 2

Calculate the stress intensity factor and formation energy of a crack $a\,c \leq r \leq a, \theta = 0$ in the disc $0 \leq r \leq a$, $0 \leq \theta \leq a$, $0 \leq \theta \leq 2\pi$ when the circumference is traction free and the crack is subject to a symmetric pressure loading of the form

$$\sigma_{\theta\theta}\ (r, 0) = \sigma_{\theta\theta}\ (r, 2\pi) = -\sigma\ (r),\ a\,c \leq r \leq a.$$

3.1.1. The Solution of Problem 1.

A suitable Airy stress function for problem 1 is given by Michell[7], Eshelby[8].

$$\Psi\ (r, \theta) = a_o + b_o \ln r + c_o r^2 + d_o r^2 \ln r$$

and the corresponding stress and displacement fields by

$$\sigma_{rr}(r,\theta) = b_o r^{-2} + 2c_o + d_o(1 + 2\ln r) \tag{1.2}$$

$$\sigma_{r\theta}(r,\theta) = 0 \tag{1.3}$$

$$\sigma_{\theta\theta}(r,\theta) = -b_o r^{-2} + 2c_o + d_o(3 + 2\ln r) \tag{1.4}$$

$$u_r(r,\theta) = E^{-1}\left\{-b_o(1+\nu)r^{-1} + 2c_o(1-\nu)r + 2d_o(1-\nu)r\ln r - d_o(1+\nu)r\right\} \tag{1.5}$$

and

$$u_\theta(r,\theta) = 4E^{-1} d_o r\theta \tag{1.6}$$

Since the solution is required to satisfy the conditions

(i) $\sigma_{rr}(a,\theta) = \sigma_{r\theta}(a,\theta) = 0, 0 \le \theta \le 2\pi$, (ii) $u_\theta(r, 2\pi) = r\Omega$ and

(iii) u_r and u_θ are bounded at $r = 0$, we see that $b_o = 0$, $d_o = E\Omega/8\pi$ and $c_o = -(E\Omega/8\pi)\ln(a\sqrt{e})$. Therefore,

$$\Psi(r,\theta) = \frac{E\Omega}{8\pi} r^2 \ln(r/a\sqrt{e}) \tag{1.7}$$

and

$$\sigma_{\theta\theta}(r,0) = \frac{E\Omega}{4\pi}\left\{1 + \ln(r/a)\right\} \tag{1.8}$$

It follows that we may write $\sigma(r) = p_o f(r/a)$ where

$$p_o = E\Omega/4\pi \text{ and } f(\rho) = 1 + \ln\rho .$$

3.1.2. The Solution of Problem 2

If we introduce the dimensionless quantities $\rho = r/a$ (already introduced)

$$s_{\rho\rho}(\rho,\theta) = \frac{\sigma_{rr}(r,\theta)}{p_o}, \quad s_{\rho\theta}(\rho,\theta) = \frac{\sigma_{r\theta}(r,\theta)}{p_o}, \quad s_{\theta\theta}(\rho,\theta) = \frac{\sigma_{\theta\theta}(r,\theta)}{p_o} \tag{2.1}$$

$$u(\rho,\theta) = \frac{E\,u_r(r,\theta)}{p_o(1+\nu)a} \quad \text{and} \quad v(\rho,\theta) = \frac{E\,u_\theta(r,\theta)}{p_o(1+\nu)a},$$

then, by making use of a symmetry argument, it is easily shown that problem 2 may be stated as follows:

Solve the dimensionless, plane stress equations of elasticity in the semi-disc $0 \leq \rho \leq 1$, $0 \leq \theta \leq \pi$ subject to the conditions

(i) The stresses and displacements are bounded at $r = 0$.

(ii) $s_{\rho\rho}(1,\theta) = s_{\rho\theta}(1,\theta) = 0$, $0 \leq \theta \leq \pi$

(iii) $s_{\rho\theta}(\rho,0) = s_{\rho\theta}(\rho,\pi) = 0$, $0 \leq \rho \leq 1$

(iv) $v(\rho,\pi) = 0$, $0 \leq \rho \leq 1$

(v) $v(\rho,0) = 0$, $0 \leq \rho \leq c$

(vi) $s_{\theta\theta}(\rho,0) = -(1 + \log \rho)$, $c \leq \rho \leq 1$

(vii) $\lim_{\rho \to 1-} \frac{\partial v(\rho,0)}{\partial \rho} < \infty$

By slightly modifying the results in section 2 of Tweed and Rooke [9] it can be shown that there is a solution of the equations of elasticity, in the given region, which satisfies the conditions (i) through (v) and is such that

$$s_{\theta\theta}(\rho,0) = \frac{1}{\pi} \int_c^1 \frac{P(t)\, M(\rho,t)\,dt}{\sqrt{[(1-t)(t-c)]}} \quad , \quad 0 \leq \rho \leq 1 \tag{2.2}$$

and

$$v(\rho,0) = \frac{2}{1+\nu} \int_c^\rho \frac{P(t)\,dt}{\sqrt{[(1-t)(t-c)]}} \quad , \quad c \leq \rho \leq 1 \tag{2.3}$$

where $P(t)$ is an arbitrary function of t

and

$$M(\rho,t) = \frac{1}{t-\rho} + \frac{(t^2-1)^2}{t(1-\rho t)^3} + \frac{t(t^2-1)}{(1-\rho t)^2} - \frac{t}{(1-\rho t)} + t - \frac{1}{t} \tag{2.4}$$

It follows that conditions (vi) and (vii) will be satisfied also if $P(t)$ is a solution of the singular integral equation

$$\frac{1}{\pi} \int_c^1 \frac{P(t)\, M(\rho,t)\,dt}{\sqrt{[(1-t)(t-c)]}} = -(1 + \log \rho) \ , \ c < \rho < 1 \tag{2.5}$$

with subsidiary condition

$$P(1) = 0 \tag{2.6}$$

3.1.3 The Stress Intensity Factor and Crack Energy

The stress intensity factor K_I and the crack formation energy W are defined by the equations

$$K_I = \lim_{r \to ac+} \sqrt{2\pi (r - ac)} \; \frac{E}{2} \; \frac{\partial u_\vartheta}{\partial r}(r, 0) \tag{3.1}$$

and

$$W = \int_{ac}^{a} p_o \left[1 + \log(r/a)\right] u_\vartheta (r, 0)\, dr \tag{3.2}$$

respectively. Therefore, by (3.1) and (3.2), we see that

$$K_I = p_o \sqrt{\frac{2\pi a}{1 - c}} \; P(c) \quad , \tag{3.3}$$

and

$$W = - \frac{2 p_o^2 a^2}{E} \int_c^1 \frac{t\, P(t) \log t}{\sqrt{\left[(1-t)(t-c)\right]}}\, dt \tag{3.4}$$

Let K_o and W_o be the stress intensity factor and formation energy respectively of a crack of length 2 (a - ac) in an infinite elastic solid, when the crack is opened by a uniform pressure p_o, then after Sneddon and Lowengrub[10]

$$K_o = p_o \sqrt{\pi a (1-c)} \tag{3.5}$$

and

$$W_o = \frac{\pi p_o^2 a^2}{E} (1-c)^2 \tag{3.6}$$

Therefore

$$\frac{K_I}{K_o} = \frac{\sqrt{2}}{1-c} P(c) \quad , \tag{3.7}$$

and

$$\frac{W}{W_o} = -\frac{2}{\pi(1-c)^2}\int_c^1 \frac{t\ P(t)\ \log t}{\sqrt{(1-t)\ (t-c)}}\ dt \qquad (3.8)$$

Also of interest is the strain energy release rate $\mathcal{G}(\ell)$ which is defined by

$$\mathcal{G}(\ell) = \frac{\partial W}{\partial \ell} = \frac{1}{E}\ K_I^2 \qquad (3.9)$$

where $\ell = a\ (1-c)$ is the crack length

If we define

$$\mathcal{G}_o(\ell) = \frac{1}{E}\ K_o^2 = \frac{p_o^2\ \pi\ a\ (1-c)}{E} \qquad (3.10)$$

then

$$\frac{\mathcal{G}}{\mathcal{G}_o} = \frac{K_I^2}{K_o^2} = \frac{2}{(1-c)^2}\ P^2\ (c) \qquad (3.11)$$

3.1.4 Numerical Procedure

The equations (2.5) and (2.6) are solved numerically by a Gauss-Chebyshev quadrature technique which is due to Erdogan and Gupta[11]. This involves setting $x_i = \cos[(2i-1)\pi/2N]$, $t_i = \frac{1}{2}(1-c)\ x_i + \frac{1}{2}(1+c)$, $r_j = \frac{1}{2}(1-c)\cos(j\pi/N) + \frac{1}{2}(1+c)$ $i = 1, 2, \ldots, N$; $j = 1, 2, \ldots, (N-1)$, and replacing the equations (2.5) and (2.6) by the linear algebraic system

$$\frac{1}{N}\sum_{i=1}^{N} P(t_i)\ M(r_j, t_i) = -[1 + \log r_j] \qquad (4.1)$$

$$\frac{1}{N}\sum_{i=1}^{N} P(t_i)\left(\frac{1+x_i}{1-x_i}\right)^{\frac{1}{2}}\ (-)^{i-1} = 0$$

$j = 1, 2, \ldots, (N-1)$. On solving these equations for the quantities $P(t_i)$

the ratio K_I/K_o is calculated by means of the Chebyshev-Lagrange interpolation formula

$$\frac{K_I}{K_o} = \frac{\sqrt{2}}{N(1-c)} \sum_{i=1}^{N} (-)^{i+N} \left(\frac{1-x_i}{1+x_i}\right)^{\frac{1}{2}} P(t_i) \qquad (4.2)$$

and the ratio W/W_o from the Gaussian quadrature formula

$$\frac{W}{W_o} = -\frac{2}{N(1-c)^2} \sum_{i=1}^{N} t_i \, P(t_i) \log t_i \qquad (4.3)$$

Figure 12 shows some typical crack shapes, and table 4 summarises the calculated values for K_I/K_o, W/W_o and $\mathcal{G}/\mathcal{G}_o$ respectively. As expected the accuracy begins to fall off a little as the crack tip approaches the origin. The same data are presented as graphs in figures 13, 14 and 15 respectively.

3.2 Preliminary experiments

Figure 15 suggests a basis for development of a self-stressed fracture mechanics test, namely that a starter crack with length $\ell \gtrsim 0.5\,a$ should propagate to a length corresponding to $\mathcal{G}_{Ic}$. To evaluate this concept, a number of identical test-pieces have been manufactured from the same 0.064" thick sheet of commercially pure aluminium (S 1 C) by joining the cut edges with adhesives of different but known $\mathcal{G}_{Ic}$'s. Each test-piece was cleaned and anodised using a phosphoric acid solution, in accordance with the procedures listed in Table 3.

A test-piece at various stages of manufacture is shown in Figure 16. Two punch and die operations are employed, the first to fabricate a 3" diameter disc and the second to punch a $\frac{1}{2}$" diameter central hole. A 0.006" milling cutter is then used to remove the sector; a 0.012" cut at the surface of the central hole produces a sector of angle $\Omega = 2^{o}\ 50'$ (0.05 rads). Each specimen is then shaped by pressing into a female cone, an operation which leaves sufficient space between the cut edges for insertion of a sliver of adhesive film. The gap is closed using a vice to squeeze the specimen across a chord perpendicular to the glue line, and the metal adjacent to the bond is gripped with a toolmaker's clamp until the adhesive has been cured. The bond within the limits $0.5a < r \leq a$ is removed before constraining the specimen to be flat by clamping it between $\frac{1}{2}$" thick slabs, one of plate glass in order that the crack length may be seen, and the other of mild steel.

Since the experimental cone is plastically formed, flattening introduces the in-plane stresses calculated for the elastically deformed disc, plus bending moments that are equal and opposite to the bending moments which the cone geometry would have imparted to a wholly elastic specimen. Taking $E = 70{,}000\ \text{MN m}^{-2}$, $\sigma_{\theta\theta} \sim 90\ \text{MN m}^{-2}$ at $r/a = 0.5$. This is just within the elastic limit of the aluminium used for the present experiments.

A number of tests have been carried out using each of three different adhesives for which values of $\mathcal{G}_{Ic}$ have been independently measured using conventional test methods. The data are summarised in Figure 17. As indicated by the error bars, a range of values for $\mathcal{L}$ was obtained for each material; anomalously weak joints were attributed to inadequate surface preparation and have been ignored. The stable crack length varies with the speed of testing and this is attributed to the fact that some crack propagation takes place during flattening of the cone.

These preliminary results are sufficiently encouraging to warrant a serious attempt to establish a better experimental $\mathcal{G}(\ell)$ curve than that reproduced in Figure 17. By using much thicker discs, it should be possible to manufacture self-stressed specimens without the plastic deformation operation used here, and which have a more realistic glue line width. Once a satisfactory $\mathcal{G}(\ell)$ curve has been obtained, it will be used as a calibration curve to investigate the effects of water uptake on $\mathcal{G}_{Ic}$ for a particular adhesive.

References

1. Miller, C. M., Report on proposed Aerospace Practice, 1524ARP, Society of Automotive Engineers Inc.

2. Timoshenko, S., 1947, Strength of Materials, 2nd Ed., (Van Nostrand, New York)

3. Love, A. E. H., 1959 Treatise on the Mathematical Theory of Elasticity, 4th Ed., (Cambridge University).

4. Barrer, R. M. 1941, Diffusion in and through solids (Cambridge University)

5. Farrar, N. R., and Ashbee K. H. G., 1978, J. Phys. D. 11, No. 4, 1009.

6. Harris, W. F., Scientific American, 1977, 237, 6, 130.

7. Mitchell, J. H. 1899 Proc. Lond. Math. Soc. 31, 100.

8. Eshelby J. D. 1966 Brit. J. Appl. Phys. 17, 1131 - 1135.

9. Tweed J. and Rooke D. P. 1973 Int. J. Engng. Sci. 11, 65-73.

10. Sneddon I. N. and Lowengrub M. 1969 Crack Problems in the Classical Theory of Elasticity Wiley J. and Sons N. Y.

11. Erdogan F. and Gupta, G. D. 1972 Q. Appl. Math. 29, 523.

TABLE I

Reflection coefficients

Interface	Reflection %
air/water	2
air/glass	4
water/glass	0.4
glass/resin	0.05
water/resin	0.7

Table 2

Adhesives and curing Schedules

	Resin system	Proportions	Gel	Cure
	Ciba Geigy	p.b.w.		
	MY 750 (Diglycidyl ether of bisphenol A)	100	2 hours	4 hours
A			at	at
	HY 917 (Methyl tetrahydrophthalic anhydride)	85	100°C	150°C
	DY 062 (Triamyl ammonium phenate)	2		
	Bloomingdale			1 hour
				at
	FM 1000 (Nylon modified epoxy film)			170°C
B				
	BR 1009/49 (Phenolic primer)		2 hours	1 hour
			at	at
			20°C	70°C

Table 3

Aluminium Surface Preparation

	Process	Solution	Time	Temperature
1.	Solvent clean in ultrasonic bath	Carbon Tetrachloride	5 mins	ambient
2.	Non-silicated alkaline clean	0.1N Sodium hydroxide	10 mins	ambient
3.	Immersion rinse	Tap water	2 mins	ambient
4.	Immersion rinse	Tap water	5 mins	38 - 60°C
5.	Deoxidise	Mixture of 170 ml Nitric acid 30 ml Hydrofluoric acid 800 ml distilled water	10 mins	ambient
6.	Immersion rinse	Tap water	2 mins	ambient
7.	Spray rinse	Distilled water		ambient
8.	Anodise	Mixture of 10 wt % Orthophosphoric acid	1 min (apply voltage) 2-5 min (step to 10 V)	
9.	Immersion rinse	Tap water	10 mins	ambient
10.	Spray rinse	Distilled water	2 mins	ambient
11.	Dry in air		30 mins	80°C
12.	Cool in air		120 mins	ambient

Table 4

ℓ/a	K_I/K_o	W/W_o	$\mathcal{G}/\mathcal{G}_o$	Check
0.01	1.123	0.630	1.261	1.000
0.1	1.136	0.640	1.292	1.000
0.2	1.149	0.651	1.321	1.000
0.3	1.158	0.659	1.342	1.000
0.4	1.161	0.665	1.348	1.000
0.5	1.154	0.668	1.333	1.000
0.6	1.132	0.664	1.282	1.000
0.7	1.083	0.651	1.173	1.000
0.8	0.985	0.625	0.971	1.000
0.9	0.784	0.578	0.615	1.000
0.99	0.278	0.510	0.078	0.997
0.999	0.089	0.501	0.008	0.970

Note

(i) $\ell = a(1-c)$ is the length of the crack.

(ii) As a check on the accuracy of the compution, $\frac{\partial W}{\partial \ell}$ was evaluated by numerical differentiation and the quantity check

$\frac{E}{K_1^2} \cdot \frac{\partial W}{\partial \ell}$ tabulated.

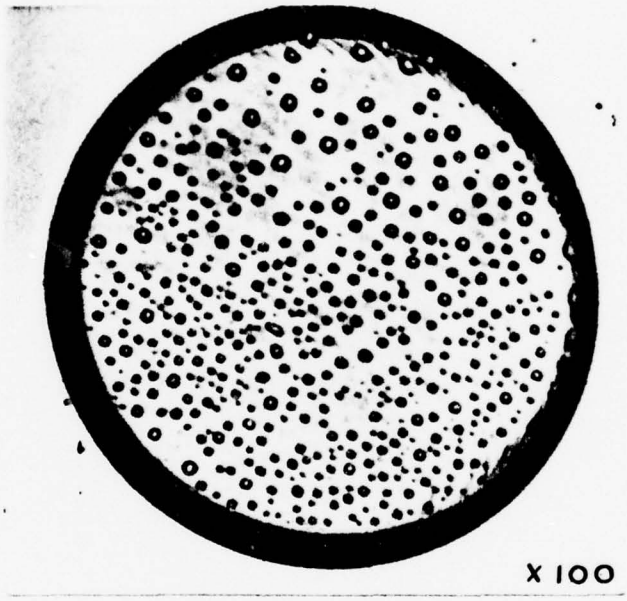

Figure 1. Condensation of diffused water inside entrapped air bubble.

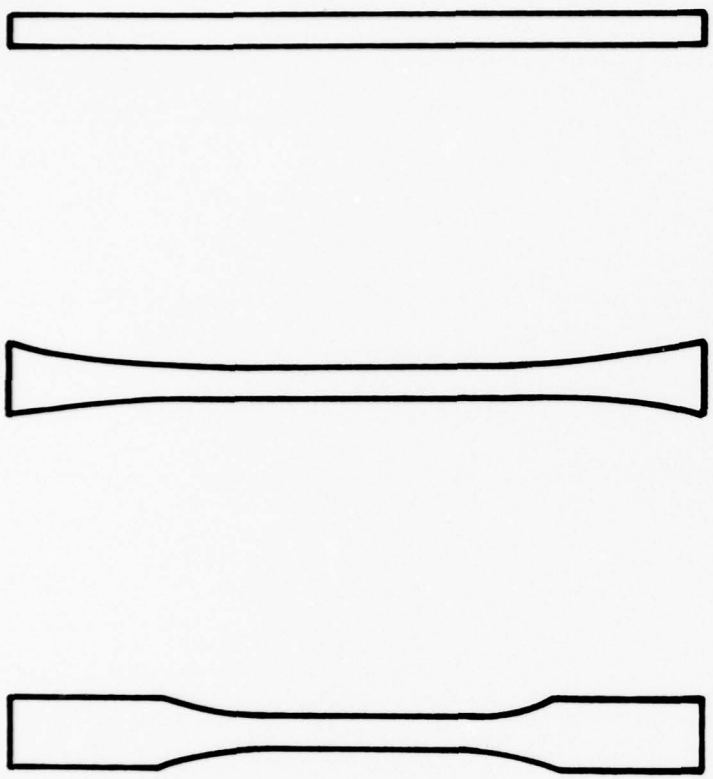

Figure 2. Inhomogeneous swelling associated with water uptake by the adhesive in a butt joint.

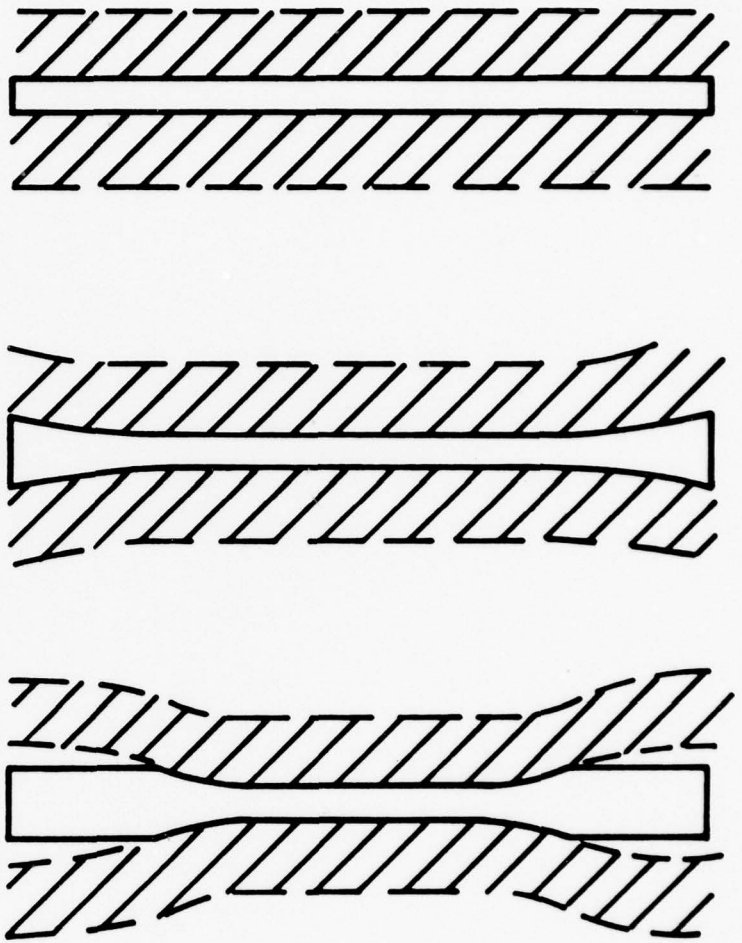

Figure 3. Same as figure 2 but with the mechanical constraint offered by the adherends.

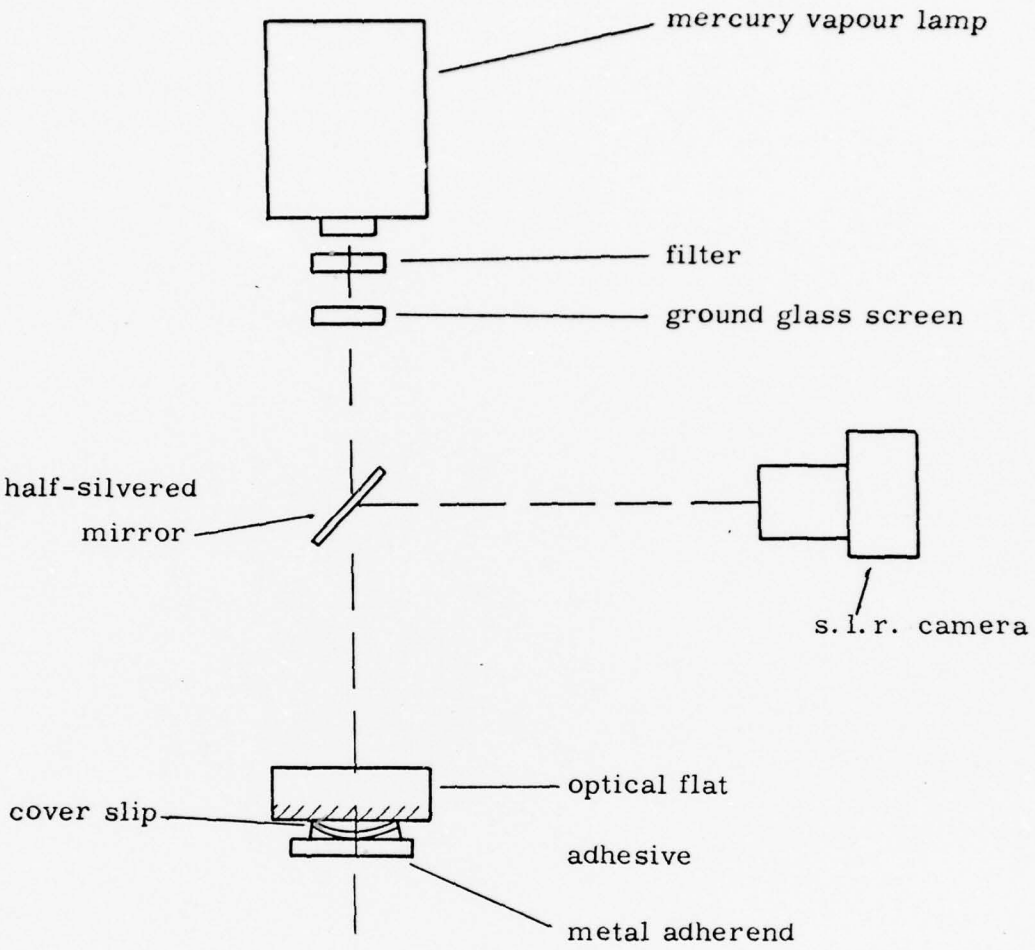

Figure 4(a) Layout of optical bench for Newton's rings experiment.

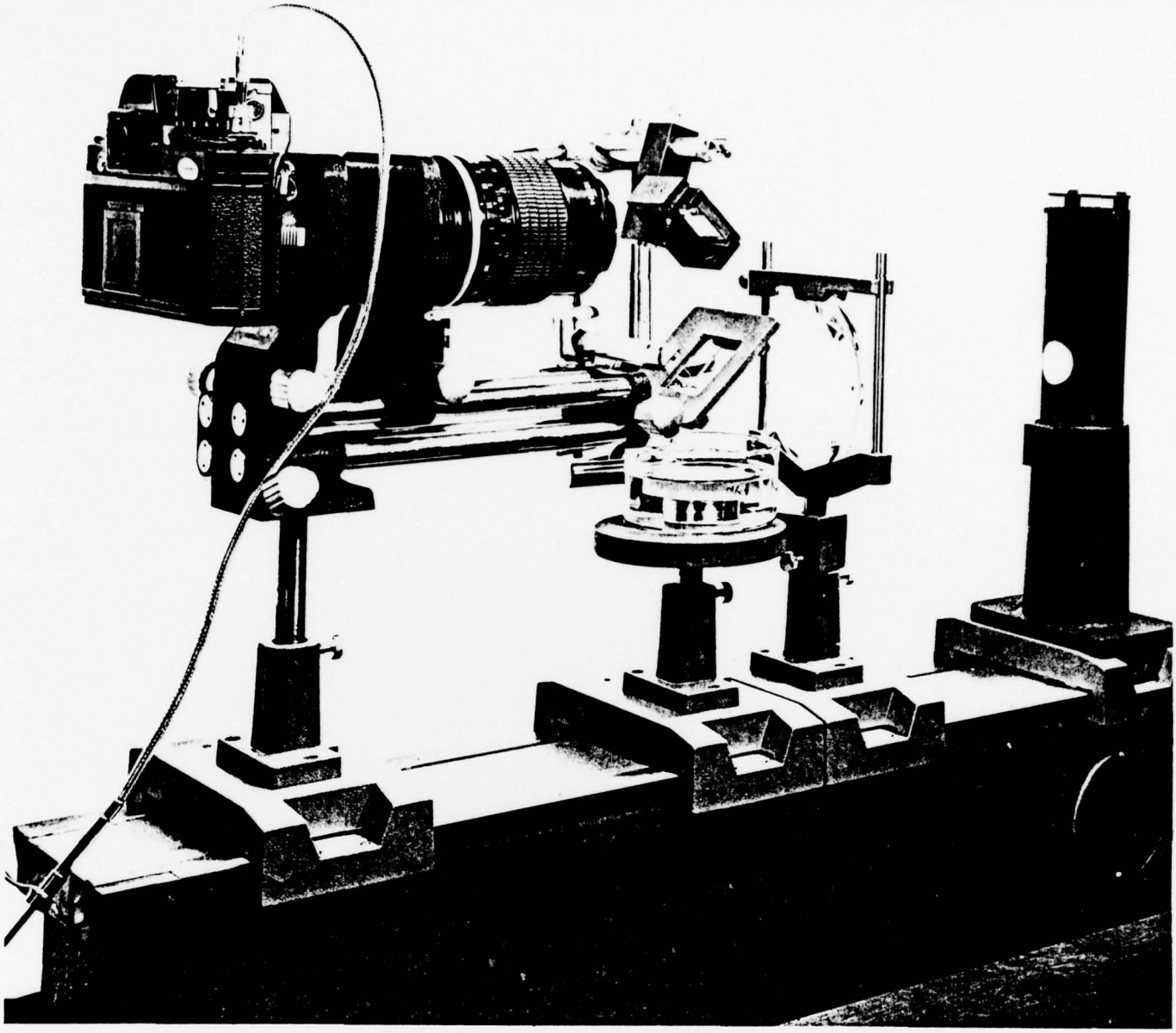

Figure 4(b) General assembly for observing and photographing the pattern of Newton's rings during exposure to room temperature water.

Figure 4(c) Close-up of the joint seen in Figure 4(b).

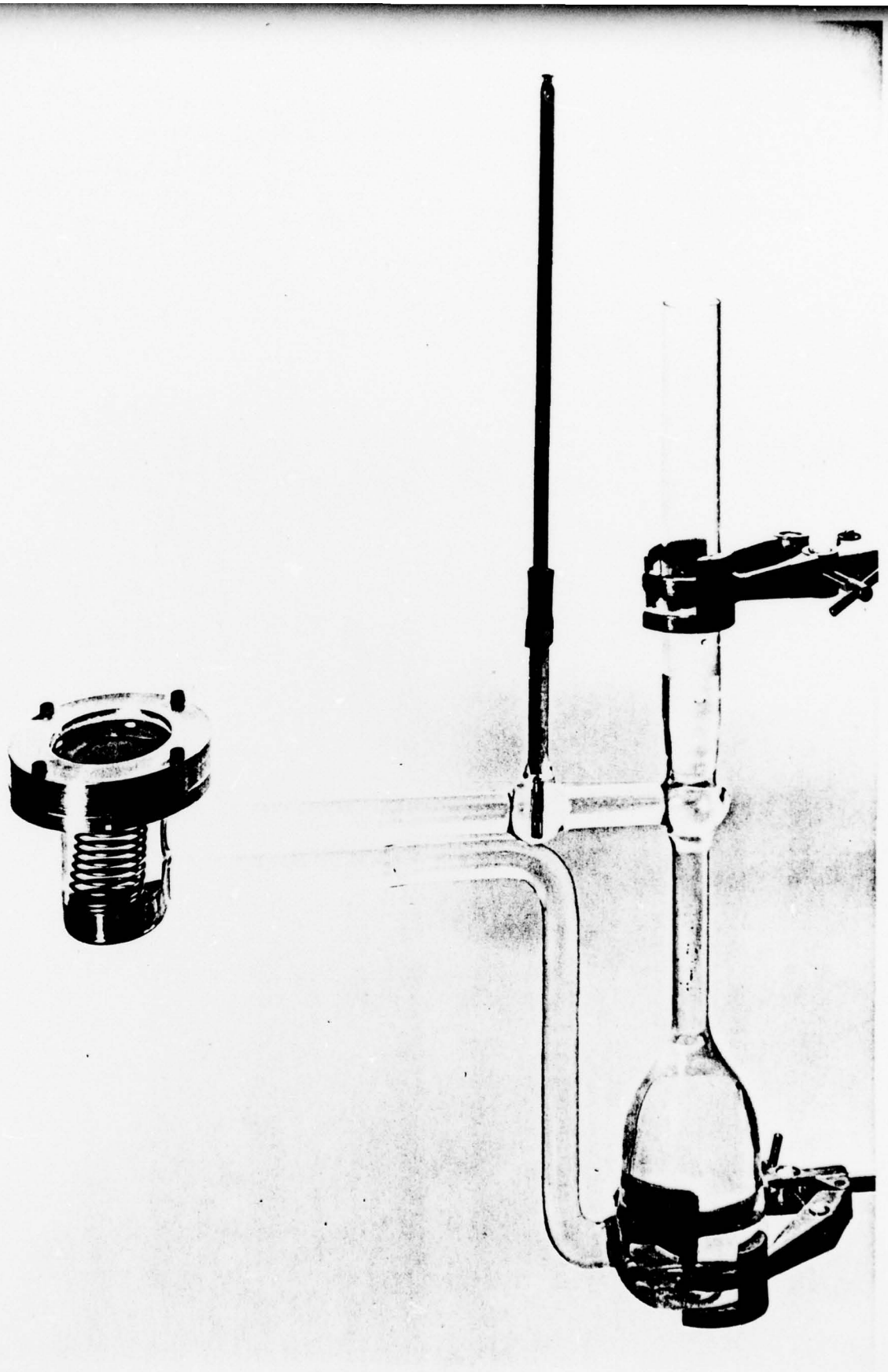

Figure 5. Apparatus developed for in situ observation of changes in the pattern of Newton's rings during swelling that accompanies the uptake of hot water. The stainless steel spring introduces a constant uniform pressure between cover slip and optical flat.

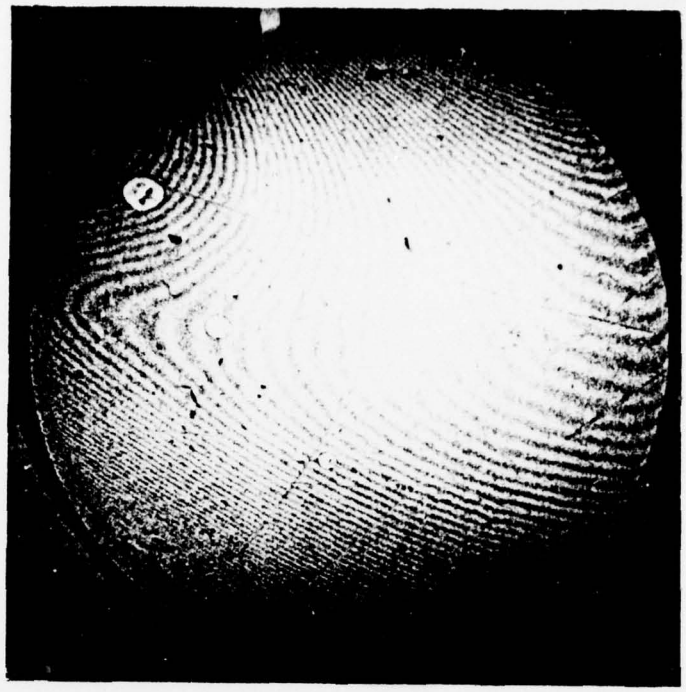

(a)

(b)

Figure 6. (a) Dual beam Newton's rings.
(b) Newton's rings produced by multiple beam interference

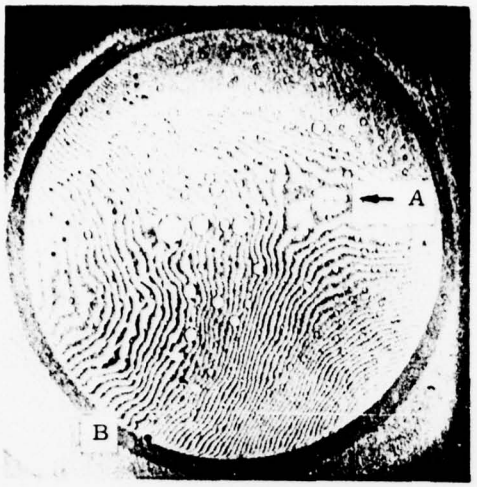

(a) BEFORE IMMERSION

(b) 116 HOURS

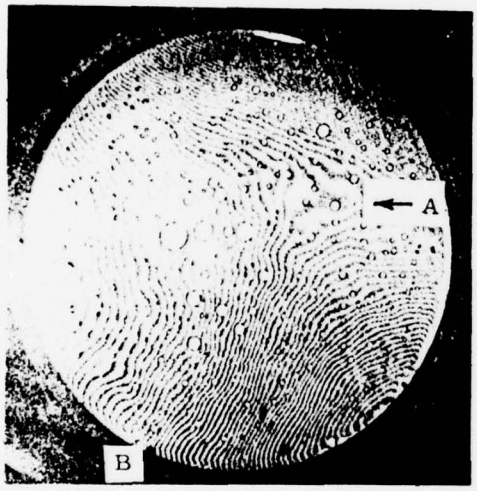

(c) 356 HOURS

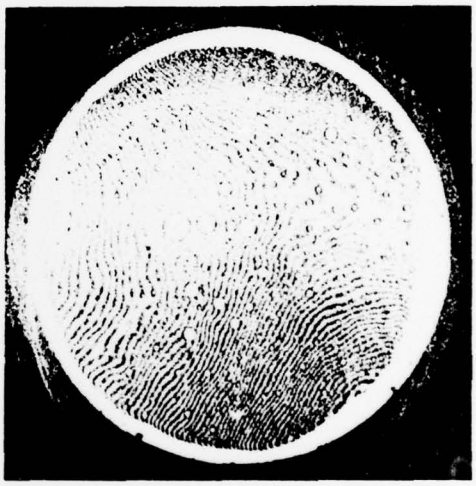

(d) 1008 HOURS

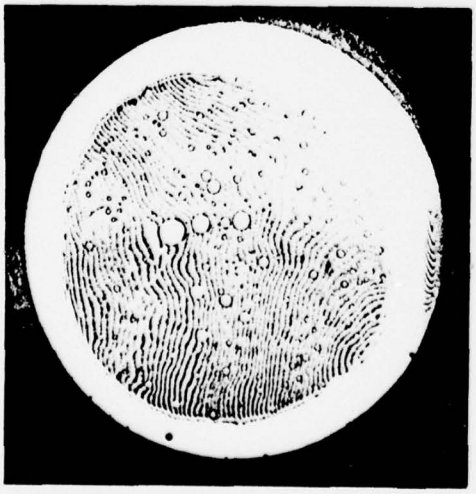

(e) 2329 HOURS

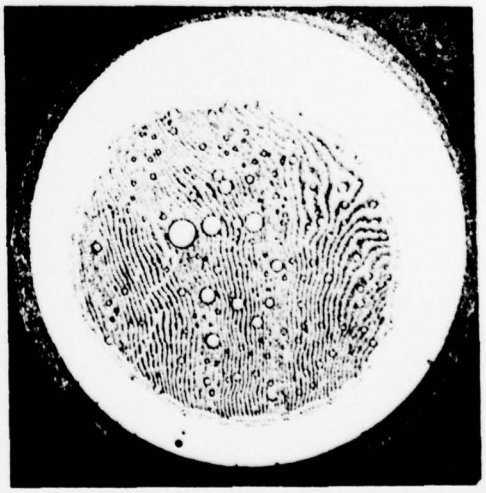

(f) 3043 HOURS

figure. 7. CHANGES IN A PATTERN OF NEWTON'S RINGS PRODUCED BY THE GAP BETWEEN AN OPTICAL FLAT AND THE OUTER SURFACE OF A GLASS COVER SLIP AS ONE ADHEREND OF A JOINT FORMED WITH AN ALUMINIUM BLOCK AND EXPOSED TO WATER AT ROOM TEMPERATURE.

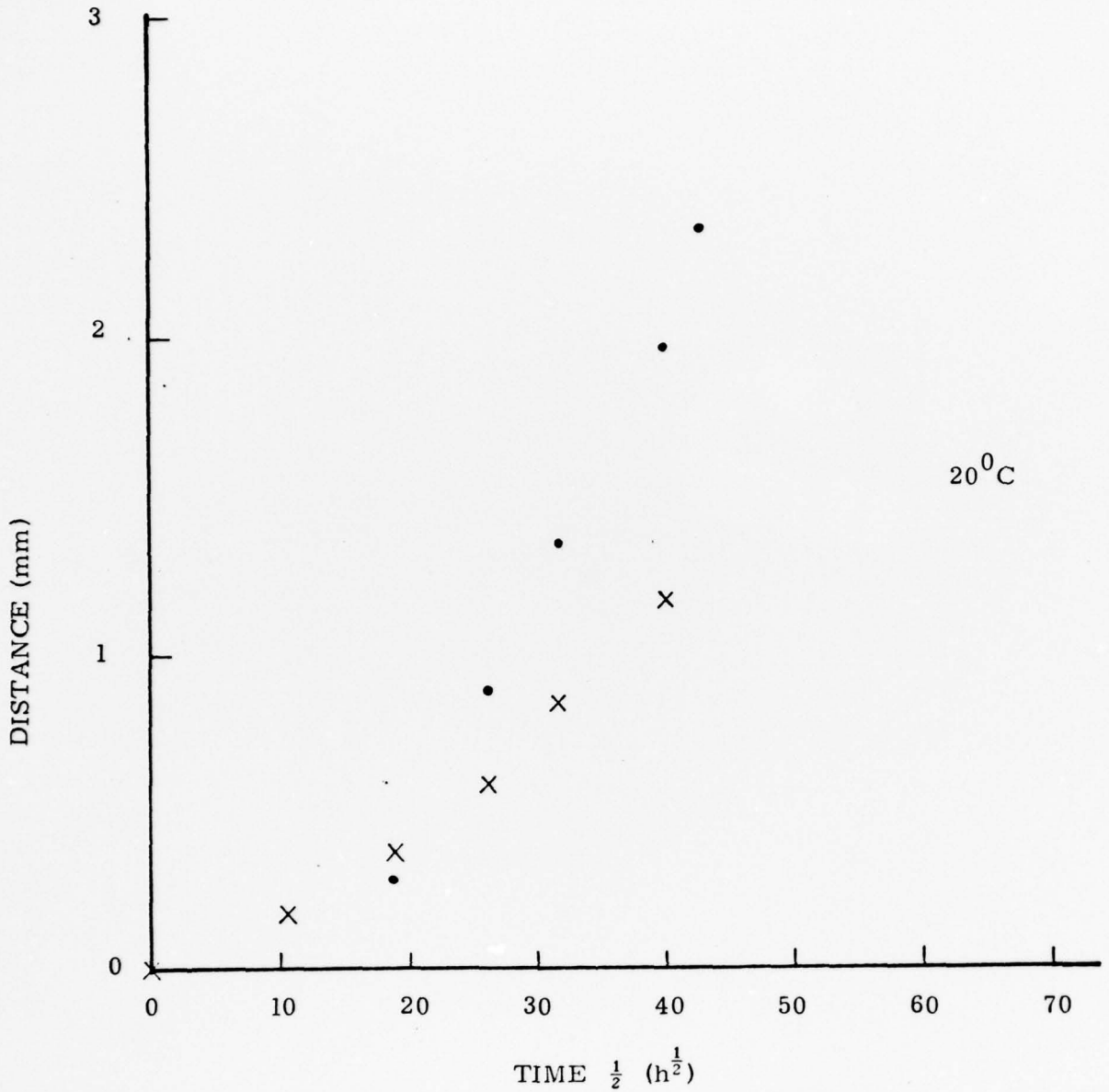

Figure 8. Distances, from the original edge of the joint shown in Figure 7, for a kink in the pattern of Newton's rings (x) and for a point on the edge of the debonding crack (•).

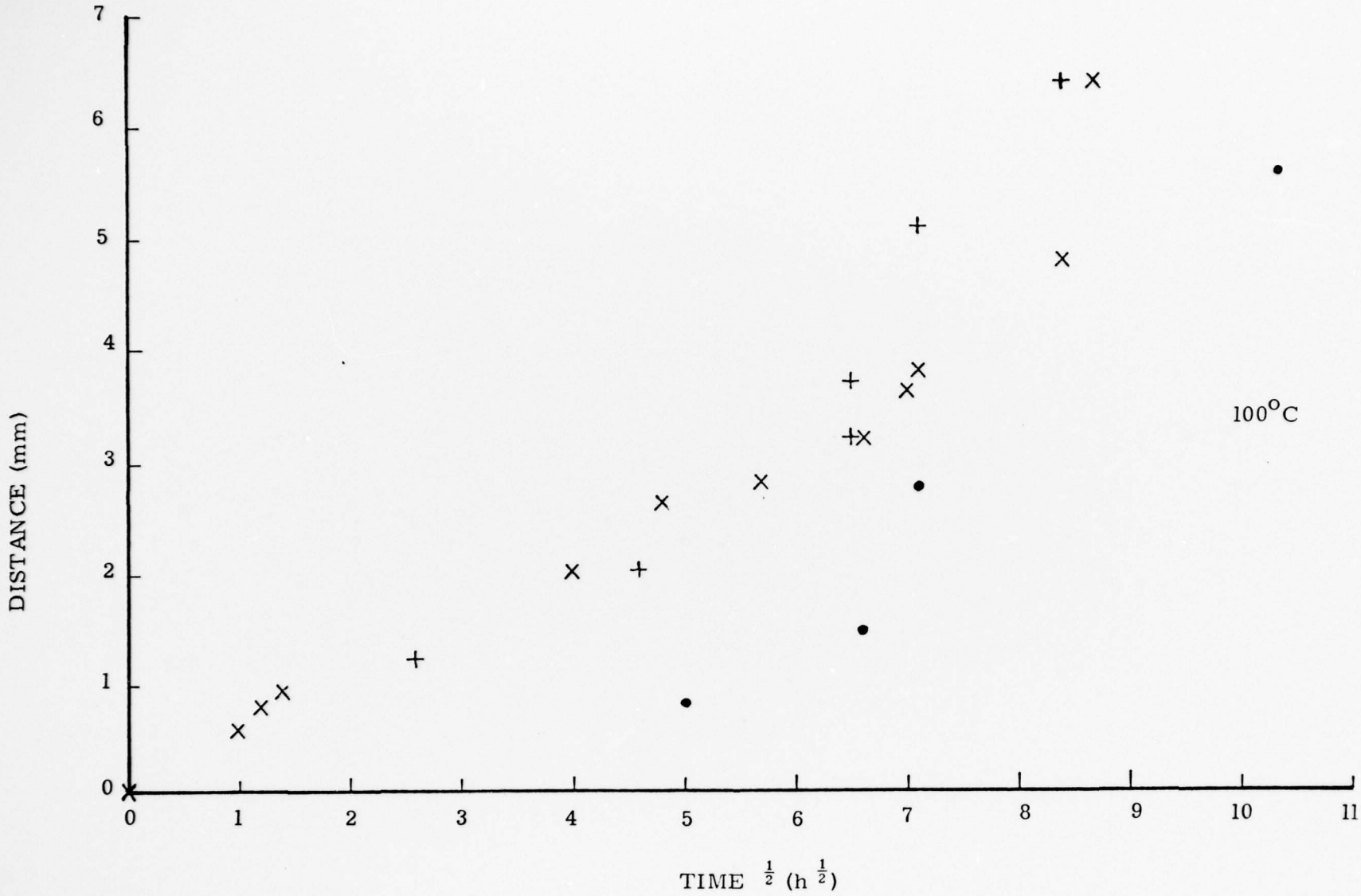

Figure 9. Distance from the original rim of a joint for the extent of saturation (X), for the debonding crack edge (•) and for water droplets inside entrapped air bubbles (+). Boiling water immersion.

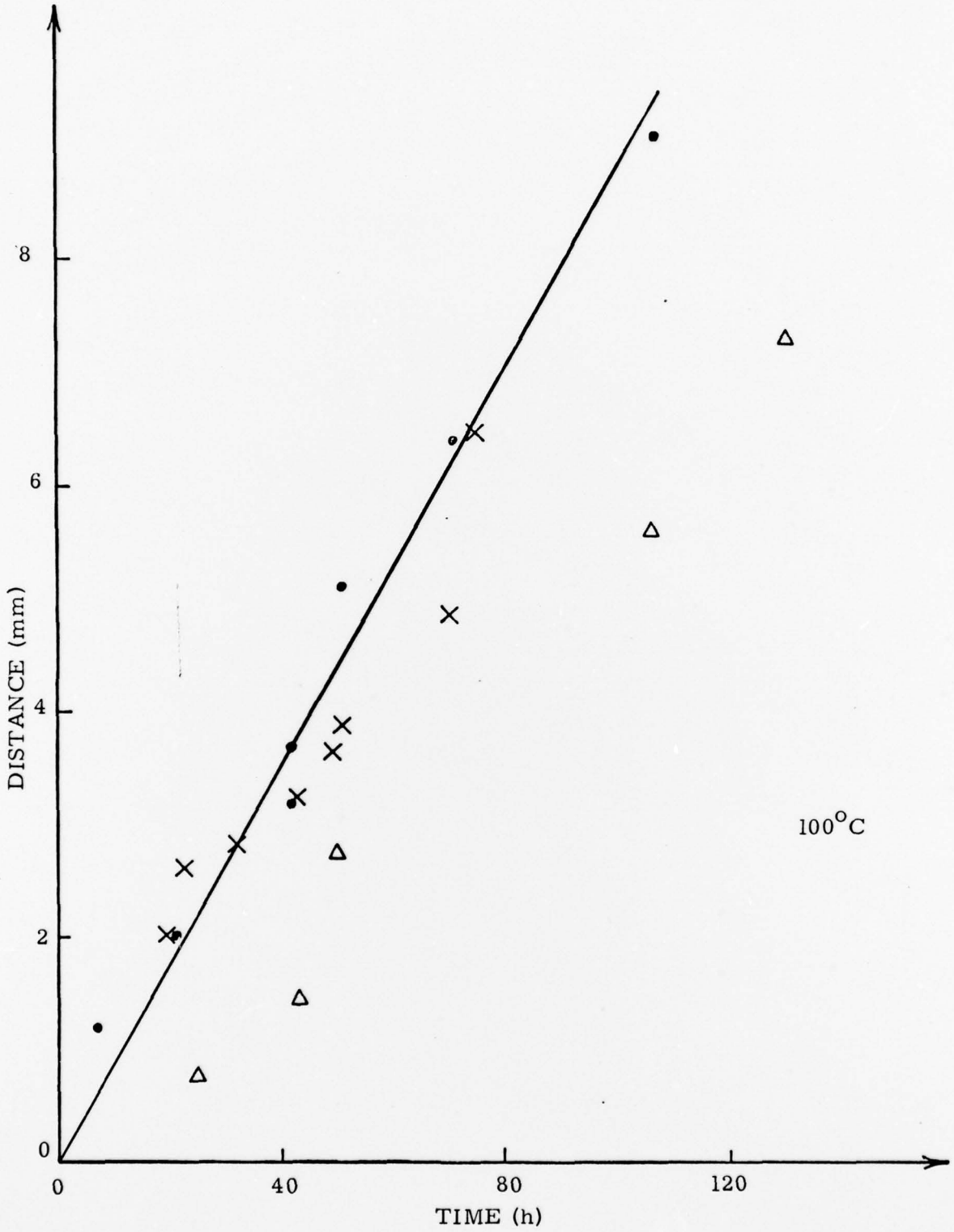

Figure 10. Variation, with time of immersion in boiling water, of the distance from the free surface of a bulk sample of resin A that is affected by internal cracking (•). Data from an adhesive joint made using the same resin and glass microscope slides are indicated by (X) for kinks in Newton's rings and by (Δ) for the edge of the debonding crack

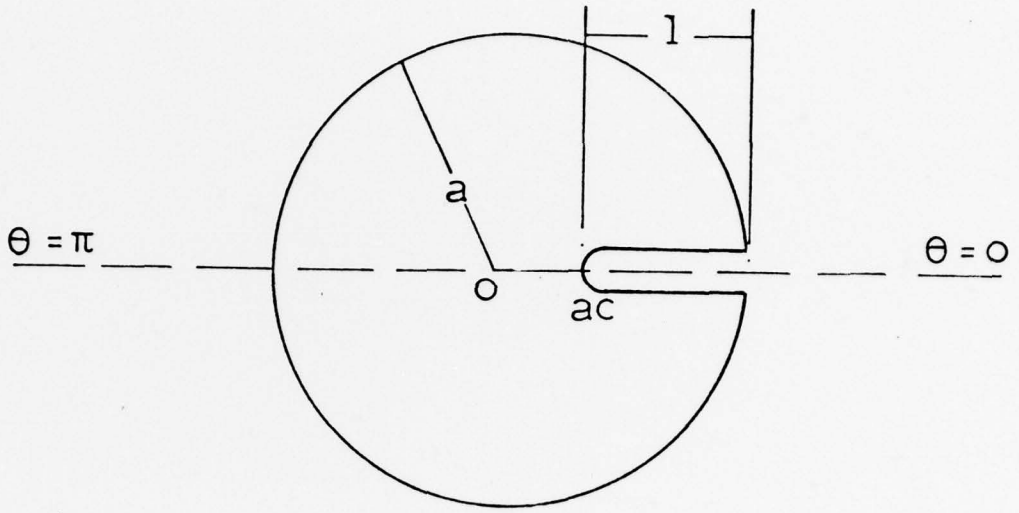

FIGURE 11 Disc containing a radial edge crack

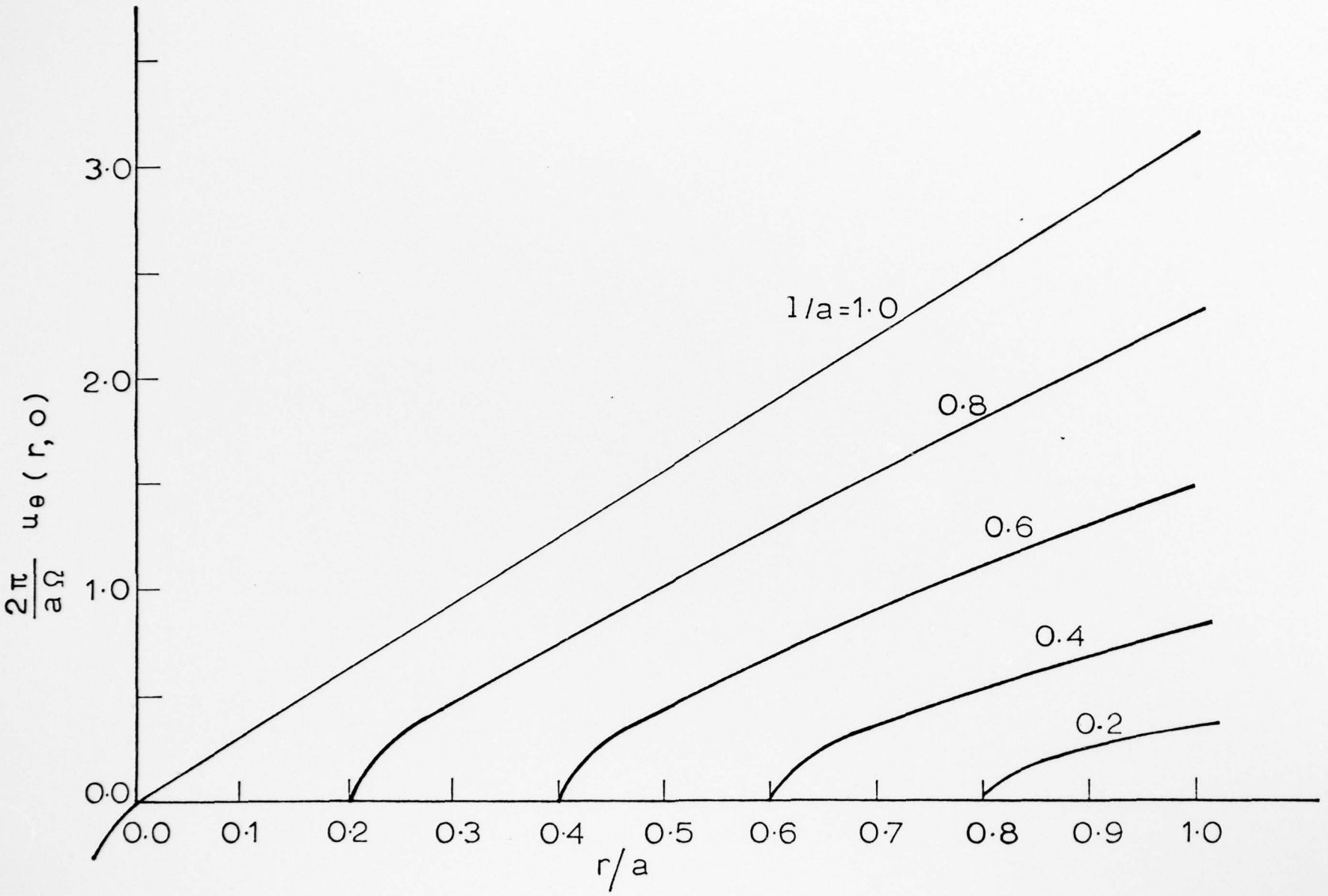

FIGURE 12 Some typical crack shapes

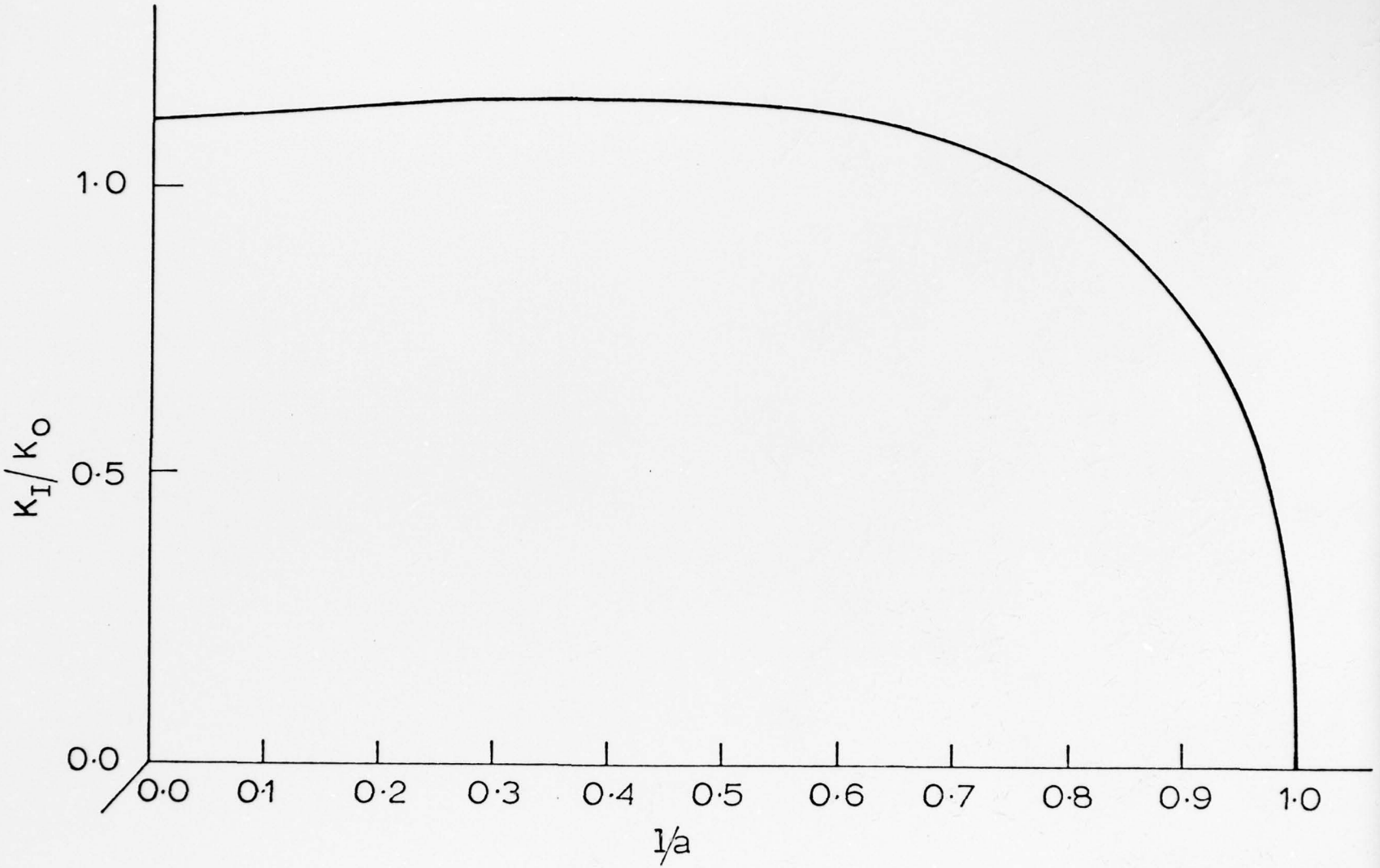

FIGURE 13 K_I/K_o versus ℓ/a ($K_o = \frac{E\delta\epsilon}{4\pi}\sqrt{\pi\ell}$)

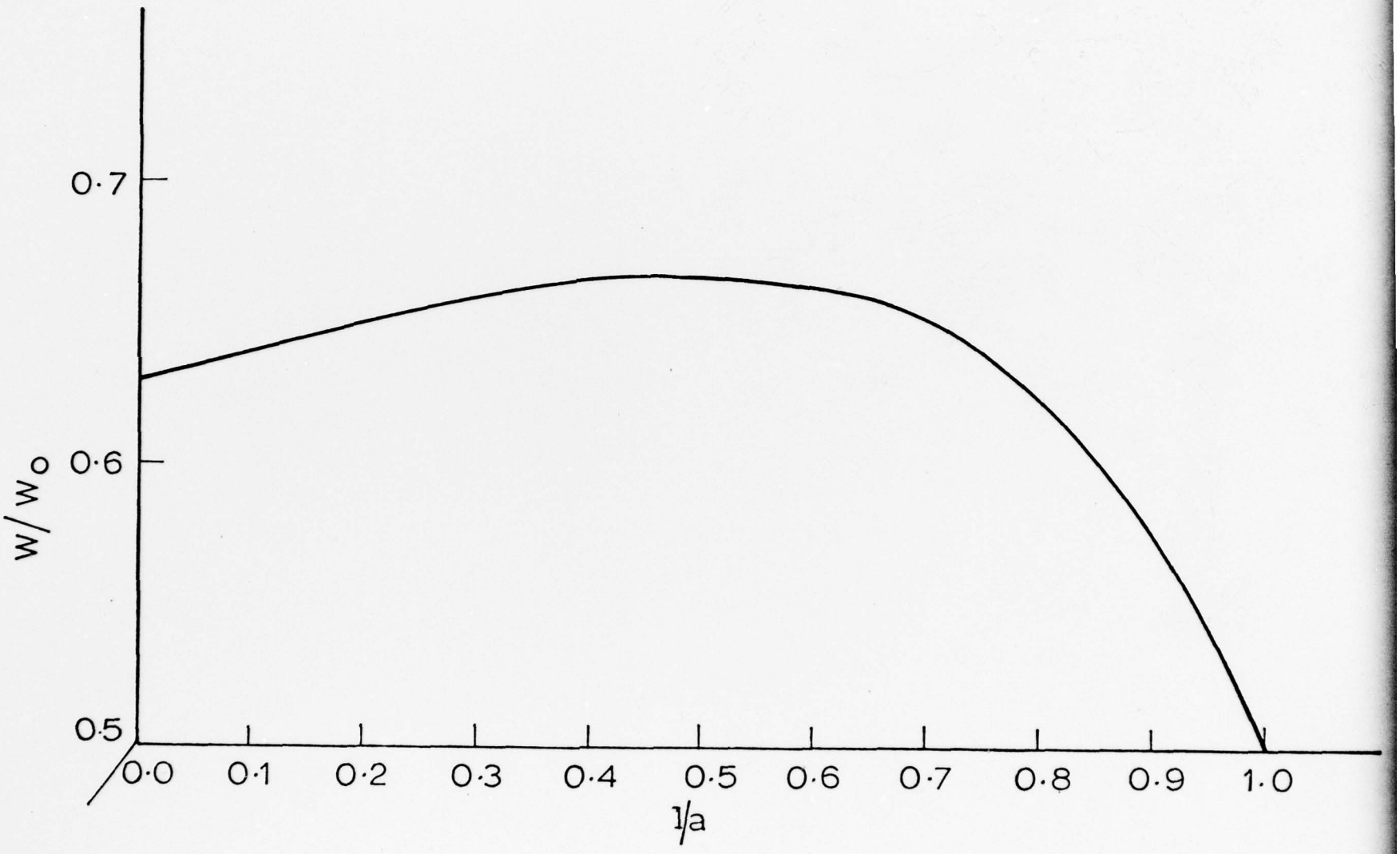

FIGURE 14 W/W_o versus ℓ/a. ($W_o = \frac{E\mathcal{N}^2}{16\,\pi}\,\ell^2$)

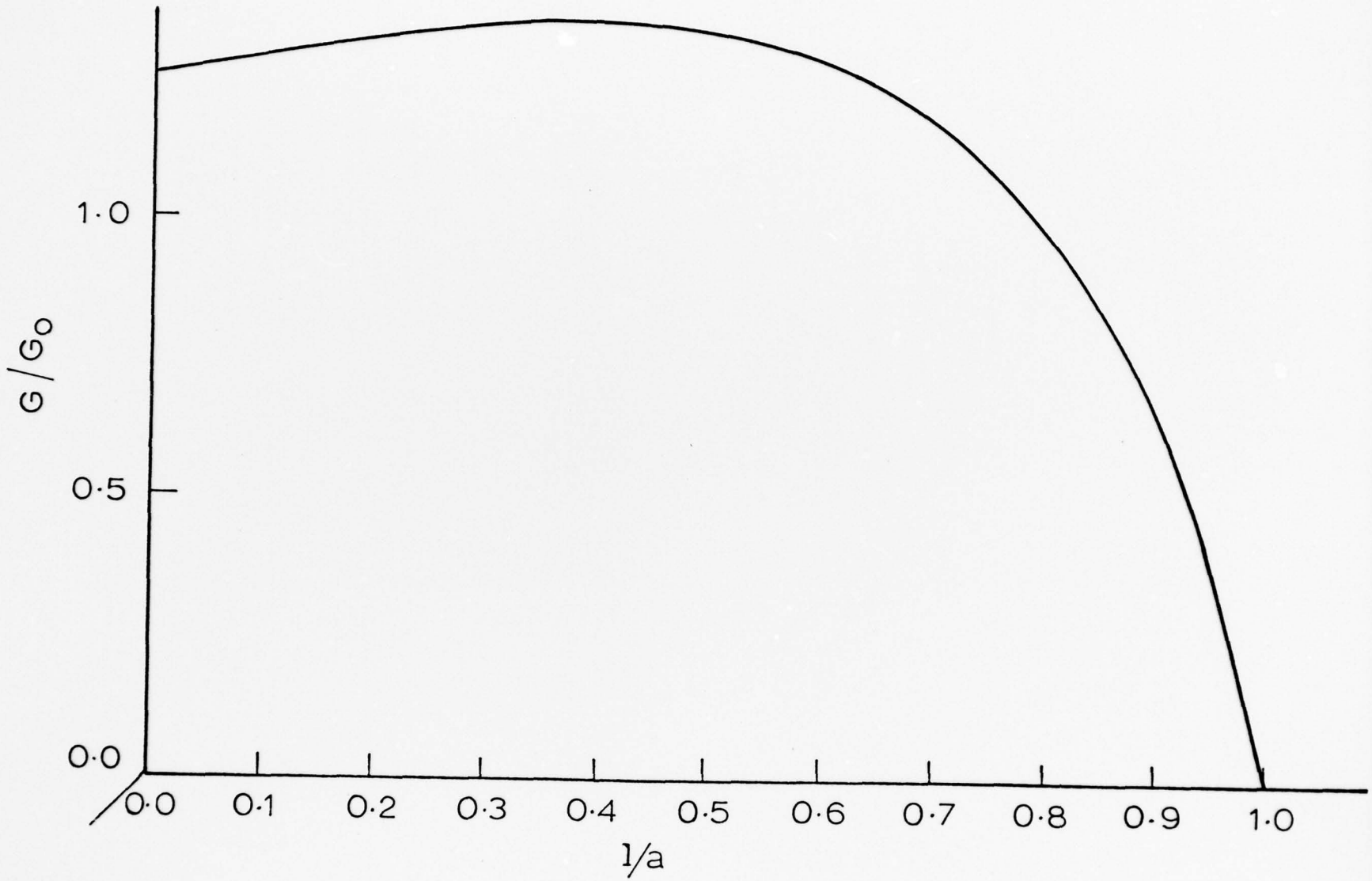

FIGURE 15 $\mathcal{G}/\mathcal{G}_o$ versus ℓ/a. ($\mathcal{G}_o = \frac{E\delta^2}{16\pi}\ell$)

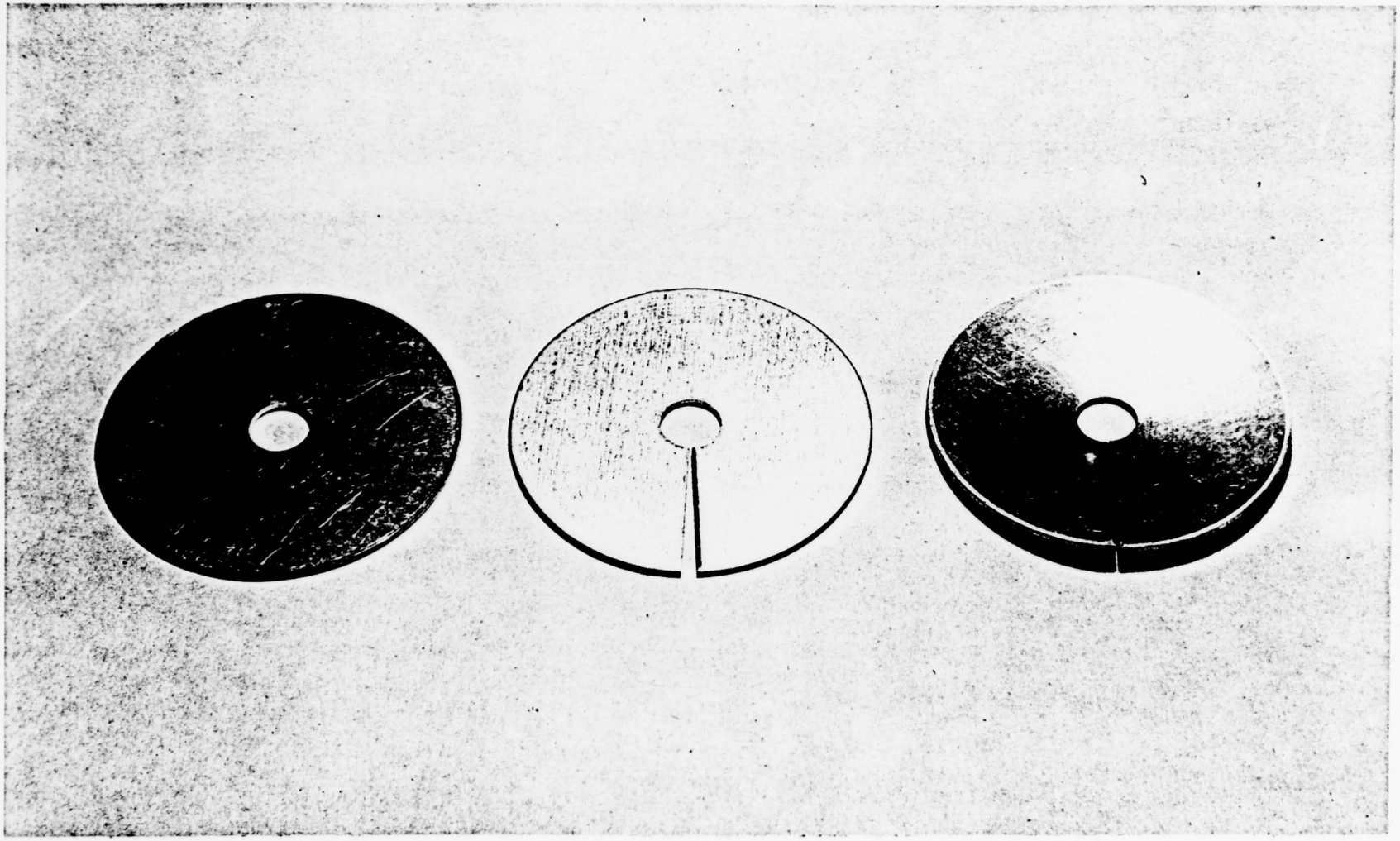

FIGURE 16. Successive stages in the manufacture of a self-stressed fracture mechanics test-piece from 16 gauge (0.064" thick) aluminium sheet.

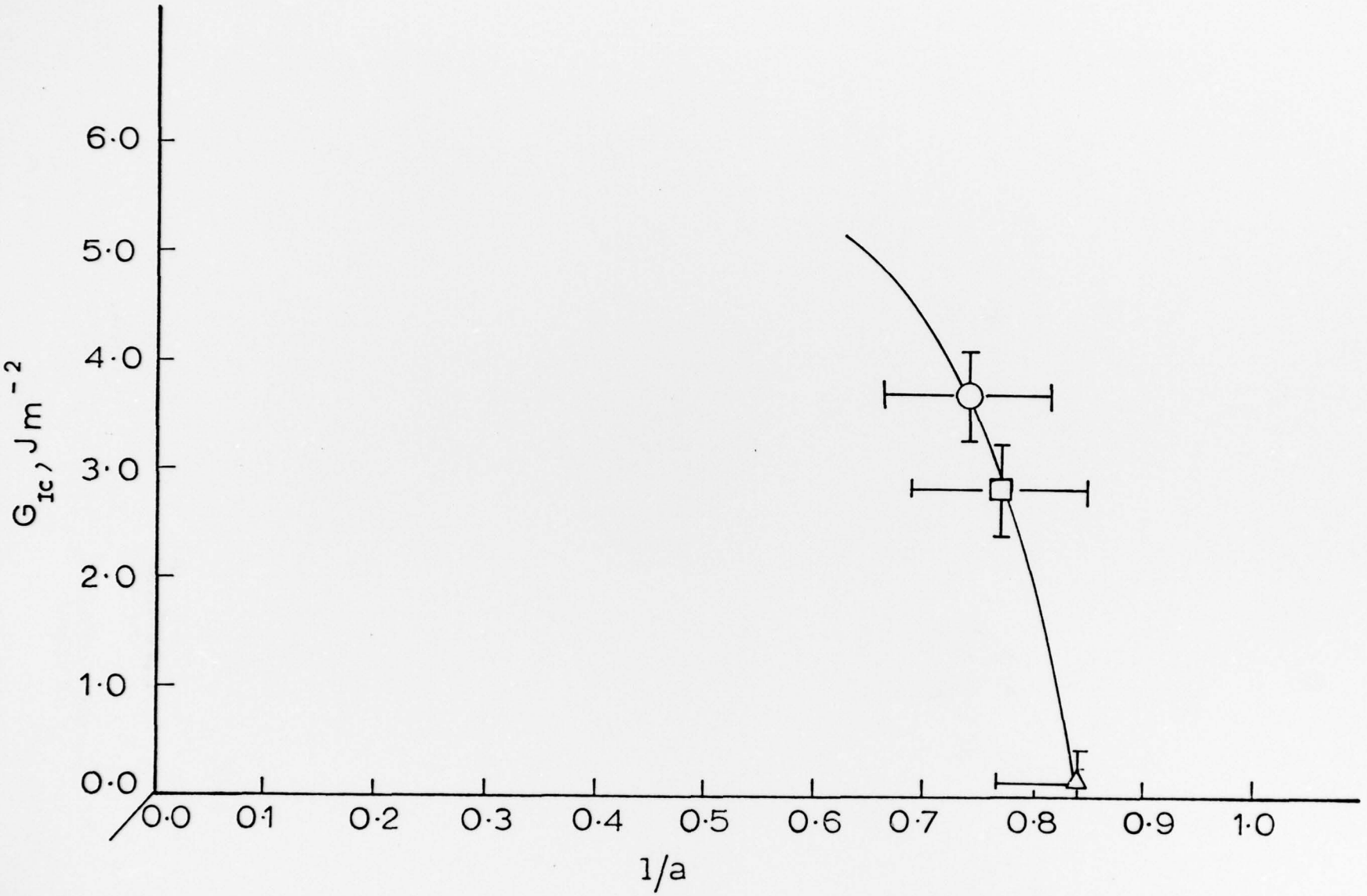

FIGURE 17 Experimental data for G_{Ic} versus l/a. ○ American Cyanamid FM 73 M, □ Ciba-Geigy BSL 312/5, △ Ciba-Geigy MY 750 with manufacturer's recommended proportions of HY 917 and DY 062.